AMERICAN SOCIETY FOR MICROBIOLOGY | Applied and Environmental Microbiology®

GEOMICROBIOLOGY

Microbe-Mineral Interactions between Asbestos and Thermophilic Chemolithoautotrophic Anaerobes

Jessica K. Choi,[a]* Ruggero Vigliaturo,[a]§ Reto Gieré,[a,b] Ileana Pérez-Rodríguez[a]

[a]Department of Earth and Environmental Science, University of Pennsylvania, Philadelphia, Pennsylvania, USA
[b]Center of Excellence in Environmental Toxicology, University of Pennsylvania, Philadelphia, Pennsylvania, USA

ABSTRACT The Fe content and the morphometry of asbestos are two major factors linked to its toxicity. This study explored the use of microbe-mineral interactions between asbestos (and asbestos-like) minerals and thermophilic chemolithoautotrophic microorganisms as possible mineral dissolution treatments targeting their toxic properties. The removal of Fe from crocidolite was tested through chemolithoautotrophic Fe(III) reduction activities at 60°C. Chrysotile and tremolite-actinolite were tested for dissolution and potential release of elements like Si and Mg through biosilicification processes at 75°C. Our results show that chemolithoautotrophic Fe(III) reduction activities by *Deferrisoma palaeochoriense* were supported with crocidolite as the sole source of Fe(III) used as a terminal electron acceptor during respiration. Microbial Fe(III) reduction activities resulted in higher Fe release rates from crocidolite in comparison to previous studies on Fe leaching from crocidolite through Fe assimilation activities by soil fungi. Evidence of biosilicification in *Thermovibrio ammonificans* did not correspond with increased Si and Mg release from chrysotile or tremolite-actinolite dissolution. However, overall Si and Mg release from chrysotile into our experimental medium outmatched previously reported capabilities for Si and Mg release from chrysotile by fungi. Differences in the profiles of elements released from chrysotile and tremolite-actinolite during microbe-mineral experiments with *T. ammonificans* underscored the relevance of underlying crystallochemical differences in driving mineral dissolution and elemental bioavailability. Experimental studies targeting the interactions between chemolithoautotrophs and asbestos (or asbestos-like) minerals offer new access to the mechanisms behind crystallochemical mineral alterations and their role in the development of tailored asbestos treatments.

IMPORTANCE We explored the potential of chemosynthetic microorganisms growing at high temperatures to induce the release of key elements (mainly iron, silicon, and magnesium) involved in the known toxic properties (iron content and fibrous mineral shapes) of asbestos minerals. We show for the first time that the microbial respiration of iron from amphibole asbestos releases some of the iron contained in the mineral while supporting microbial growth. Another microorganism imposed on the two main types of asbestos minerals (serpentines and amphiboles) resulted in distinct elemental release profiles for each type of asbestos during mineral dissolution. Despite evidence of microbially mediated dissolution in all minerals, none of the microorganisms tested disrupted the structure of the asbestos mineral fibers. Further constraints on the relationships between elemental release rates, amount of starting asbestos, reaction volumes, and incubation times will be required to better compare asbestos dissolution treatments studied to date.

KEYWORDS microbe-mineral interactions, asbestos minerals, microbial iron reduction, thermophiles, biosilicification

Editor Jennifer B. Glass, Georgia Institute of Technology

Address correspondence to Ileana Pérez-Rodríguez, ileperez@sas.upenn.edu.

*Present address: Jessica K. Choi, Department of Ecology and Evolutionary Biology, University of Michigan, Ann Arbor, Michigan, USA.

§Present address: Ruggero Vigliaturo, Department of Earth Sciences and the Interdepartmental Centre for Studies on Asbestos and Other Toxic Particulates, University of Turin, Turin, Italy.

The authors declare no conflict of interest.

Received 13 December 2022
Accepted 6 March 2023

Asbestos is a term referring to six types of naturally occurring mineral fibers (classified as either serpentines or amphiboles) that are or have been commercially exploited (1) due to their valuable physicochemical properties, such as fire resistance, thermal stability, and low electrical conductivity (2–5). Unfortunately, the desirable physicochemical properties of asbestos are outweighed by their toxic nature when inhaled (1, 6–9). Asbestos toxicity in mammalian cells has been linked to the presence of Fe in the crystal structure and at the mineral surface, and to its active participation in oxidation-reduction (redox) reactions driving the generation of reactive oxygen species through Fenton reactions associated with the (Fe-catalyzed) Haber-Weiss cycle (10–20). The toxicity of asbestos is also linked to particle morphometry, which leads to cell puncture, frustrated phagocytosis, and inflammation propagation (9, 20–28). Structural and/or surficial Fe removal has been shown to lower Fenton-type activity involved in the generation of reactive oxygen species (29–33), whereas the removal of Mg and Si from asbestos has been shown to compromise its habit (34–37). Consequently, a variety of asbestos treatment technologies have been explored with the goal of reducing or removing the toxic properties of asbestos to enable reuse of asbestos or asbestos-containing materials as secondary raw materials (38–48) or to remediate asbestos contamination (30, 36, 49–52).

The removal of Fe via asbestos dissolution has been documented with limited success through the use of siderophores during Fe assimilation processes by lichens, soil fungi, and soil bacteria (30, 53–56). The breakdown of the asbestos habit has been shown to require high temperatures (e.g., ≥400°C [41]), thermal treatment at relatively high pressure (e.g., 300 to 700°C and 2 to 6 MPa [40]), microwave radiation (43), extreme pH conditions (38), or accelerated mechanochemical conditions (e.g., milling at 250 rpm [39]). In this study, we explored the use of microbe-mineral interactions between asbestos (and asbestos-like) minerals and anaerobic chemolithoautotrophic thermophiles as mineral dissolution treatments relevant to their crystallochemical hazards. Using the Fe-rich amphibole asbestos crocidolite [idealized general formula: $Na^2(Fe^{2+}{}_3, Fe^{3+}{}_2)Si_8O_{22}(OH)_2$ (4)], we tested the removal of Fe from asbestos through thermophilic chemolithoautotrophic Fe(III) reduction. We also tested the removal of Si and Mg from serpentine asbestos [chrysotile with idealized general formula: $Mg_3Si_2O_5(OH)_4$ (4)] and amphibole asbestos [tremolite-actinolite with idealized general formulas of $Ca_2Mg_5Si_8O_{22}(OH)_2$ for tremolite and $Ca_2(Mg, Fe^{2+})_5Si_8O_{22}(OH)_2$ for actinolite (4)] through thermophilic bacterial biosilicification processes associated with hydrothermal environments (57–60). Our results highlight potential opportunities and challenges associated with the dissolution of asbestos and asbestos-like minerals through microbe-mineral interactions with thermophilic, chemolithoautotrophic anaerobes.

RESULTS

Interactions between *Deferrisoma palaeochoriense* and crocidolite. *Deferrisoma palaeochoriense* grew with crocidolite serving as the sole source of Fe(III) as the terminal electron acceptor for chemolithoautotrophic Fe(III) reduction (Fig. 1A; see also Table S1 in the supplemental material). Final cell concentrations (average of 1.51×10^7 cells mL^{-1} by 171 h of incubation time) and doubling times (10.1 ± 0.68 h) of *D. palaeochoriense* with crocidolite were slightly lower than those obtained with $Fe(OH)_3$ as the terminal electron acceptor (average of 4.28×10^7 cells mL^{-1} by 171 h of incubation time; doubling time of 6.05 ± 0.97 h). Growth was associated with increases in dissolved Fe(II) concentrations ([Fe(II)]) of 23 ± 12 μM (at 48 h) in the presence of crocidolite and up to 0.4 ± 0.1 mM (by 122 h) in the presence of $Fe(OH)_3$ (Fig. 1A and B; Table S1). In the medium alone, neither crocidolite nor $Fe(OH)_3$ yielded increased Fe(II) concentrations in the medium over time (gray symbols in Fig. 1A and B). No significant increases in aqueous [Fe(III)] were observed for either crocidolite or $Fe(OH)_3$ in the presence or absence of microorganisms over time (Fig. S1).

An absolute [Fe(II)] increase of ~2.2 mM—from 1.78 ± 0.05 mM at 0 h to 3.96 ± 0.08 mM at 171 h—was observed from Fe extractions using unfiltered samples of crocidolite-containing cultures (Table S1). A concurrent absolute [Fe(III)] decrease of

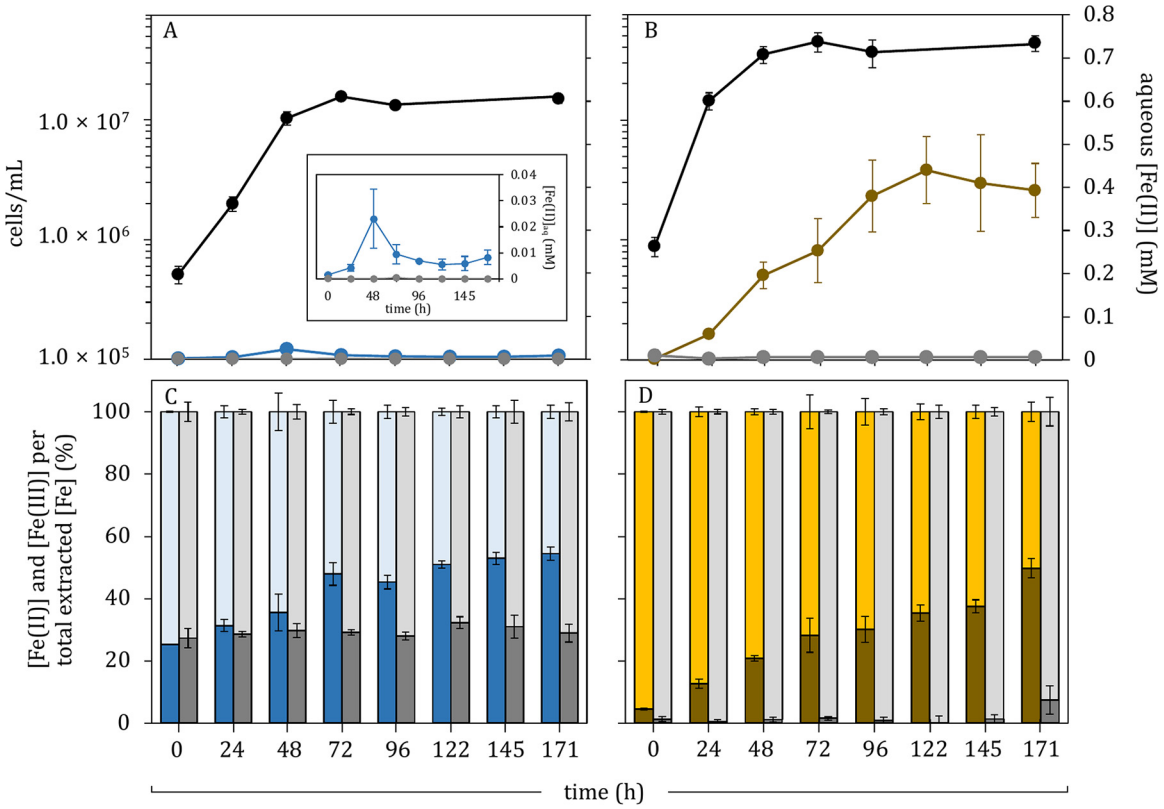

FIG 1 (A and B) Cell concentrations (black) and dissolved [Fe(II)] (blue and brown) associated with growth of *D. palaeochoriense* with (A) crocidolite or (B) $Fe(OH)_3$ as sole source of ~ 10 mM of Fe(III) for chemolithoautotrophic Fe(III) reduction. Dissolved [Fe(II)] values from mineral incubations in the medium alone are shown in gray. (C and D) Total extracted [Fe(II)] and [Fe(III)] from unfiltered samples normalized as percentages of total extracted Fe in crocidolite-containing cultures (C) and $Fe(OH)_3$-containing cultures (D). Dark blue (C) and dark brown (D) subbars represent Fe(II) values stacked below light blue (C) and gold (D) subbars representing Fe (III) values. Dark gray (C and D) subbars represent Fe(II) values stacked below light gray (C and D) subbars representing Fe(III) values associated with mineral incubations in the medium alone. All data points/bars represent averages with their standard deviations (n = 3).

~1.95 mM—from 5.27 ± 0.17 mM at 0 h to 3.32 ± 0.22 mM at 171 h—was observed in the same samples (Table S1). Normalized changes of total extractable [Fe(II)] resulted in an Fe(II) increase of ~29.2%—from 25.2% ± 0.1% Fe(II) at 0 h to 54.4% ± 2.1% Fe(II) at 171 h—in crocidolite-containing cultures (Fig. 1C). An absolute increase of ~3.0 mM [Fe(II)]—from 0.37 ± 0.03 mM at 0 h to 3.41 ± 0.63 mM at 171 h—was observed for extractions using unfiltered samples associated of $Fe(OH)_3$-containing cultures (Table S1). A concurrent absolute [Fe(III)] decrease of ~4.4 mM—from 7.82 ± 0.39 mM at 0 h to 3.39 ± 0.24 mM at 171 h—was observed in the same samples (Table S1). The ~1.4 mM difference between the Fe(II) produced and the Fe(III) reduced during microbial growth with $Fe(OH)_3$ likely reflects the production of magnetite ($Fe^{2+}Fe^{3+}{}_2O_4$), as indicated by the black magnetic precipitate resulting from chemolithoautotrophic Fe (III) reduction (61). Normalized changes of total extractable [Fe(II)] from unfiltered samples resulted in Fe(II) increase of ~45.3%—from 4.5% ± 0.3% Fe(II) at 0 h to 49.8% ± 3.1% Fe(II) at 171 h—in $Fe(OH)_3$-containing cultures (Fig. 1D). No simultaneous increase of [Fe(II)] with a decrease of [Fe(III)] was observed over time in unfiltered samples from medium incubations containing crocidolite or $Fe(OH)_3$ alone (Fig. 1C and D). Whereas $Fe(OH)_3$-containing cultures displayed an overall higher Fe(II) increase over time, the resulting Fe(II)-to-Fe(III) ratios at 171 h were similar in crocidolite- and $Fe(OH)_3$-containing cultures (Fig. 1C and D).

Total [Fe] measurements via inductively coupled plasma optical emission spectrometry (ICP-OES) analysis in filtered samples of crocidolite-containing cultures showed 138.0 ± 8.5 μM dissolved [Fe] after 48 h of incubation (from starting values of 27.6 ± 0.5 μM

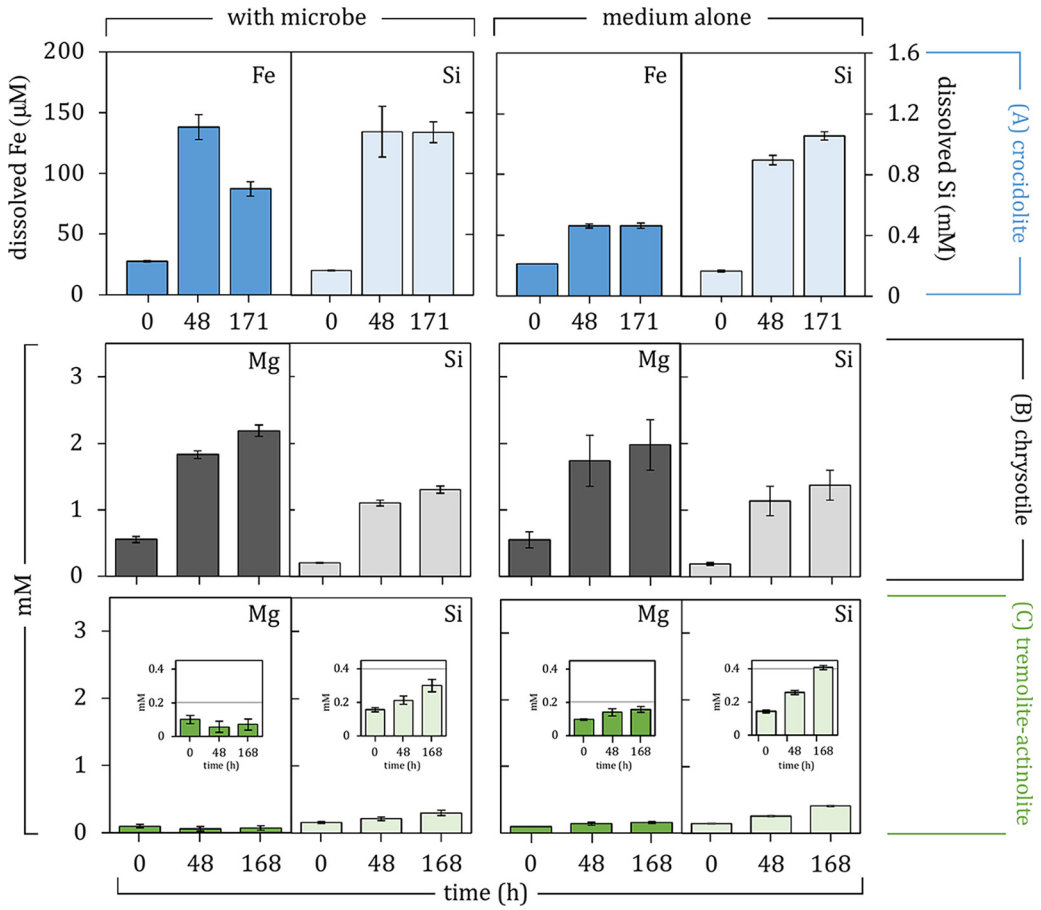

FIG 2 (A) ICP-OES measurements of dissolved [Fe] and [Si] in filtered samples of crocidolite incubations at 0, 48, and 171 h in the presence of *D. palaeochoriense* or in the medium alone. The primary *y* axis corresponds to total dissolved [Fe], whereas the secondary *y* axis corresponds to total dissolved [Si]. (B and C) ICP-OES measurements of dissolved [Mg] and [Si] in filtered samples of chrysotile (B) or tremolite-actinolite (C) incubations at 0, 48, and 168 h in the presence of *T. ammonificans* or in the medium alone. In all graphs, bars represent averages with their standard deviations ($n = 3$).

at 0 h), followed by a decrease to 87.2 ± 4.9 μM by 171 h (Fig. 2A; Fig. S2A). Only 57.6 ± 1.3 μM total dissolved [Fe] was observed via ICP-OES for crocidolite in the medium alone after 48 h (from starting values of 26.4 ± 0.0 μM at 0 h), which remained at 57.9 ± 1.8 μM dissolved Fe by 171 h of incubation at 60°C (Fig. 2A). Crocidolite's crystallinity and grain boundaries were preserved despite the observed Fe-based microbe-mineral interactions (Fig. 3A to C), and similar levels of Si release were observed after 171 h in both the presence and absence of microorganisms (Fig. 2A). The release of Si from crocidolite was 8 and 15 times higher than the amount of Fe released in culture and medium incubations after 48 h, respectively. After 171 h of incubation, the Si released from crocidolite in the cultures became 12 times higher than the Fe in solution, while the released Si in the crocidolite-containing control medium remained 15 times higher than the Fe in solution. An overall higher release of Si was observed for crocidolite-containing cultures from 24 h to 122 h of incubation, compared to crocidolite incubations in the medium alone (Fig. S3A). These observations are consistent with average bulk Fe/Si values changing from 0.60 ± 0.02 at 0 h to 0.88 ± 0.13 at 48 h and back again to 0.65 ± 0.01 at 171 h in crocidolite-containing cultures (Table S1), each assumed to represent a separate microbial population ($n = 3$). Bulk Fe/Si values of mineral particles collected from crocidolite incubations in the medium alone averaged 0.59 ± 0.02 over the entire incubation period (Table S1). The original bulk Fe/Si value for crocidolite has been reported to be 0.78 (62).

Interactions of *Thermovibrio ammonificans* with chrysotile and tremolite-actinolite. Chrysotile-containing medium and cultures resulted in the same levels of Si and Mg release over time (Fig. 2B; Table S1) despite evidence of biosilicification by *T. ammonificans*

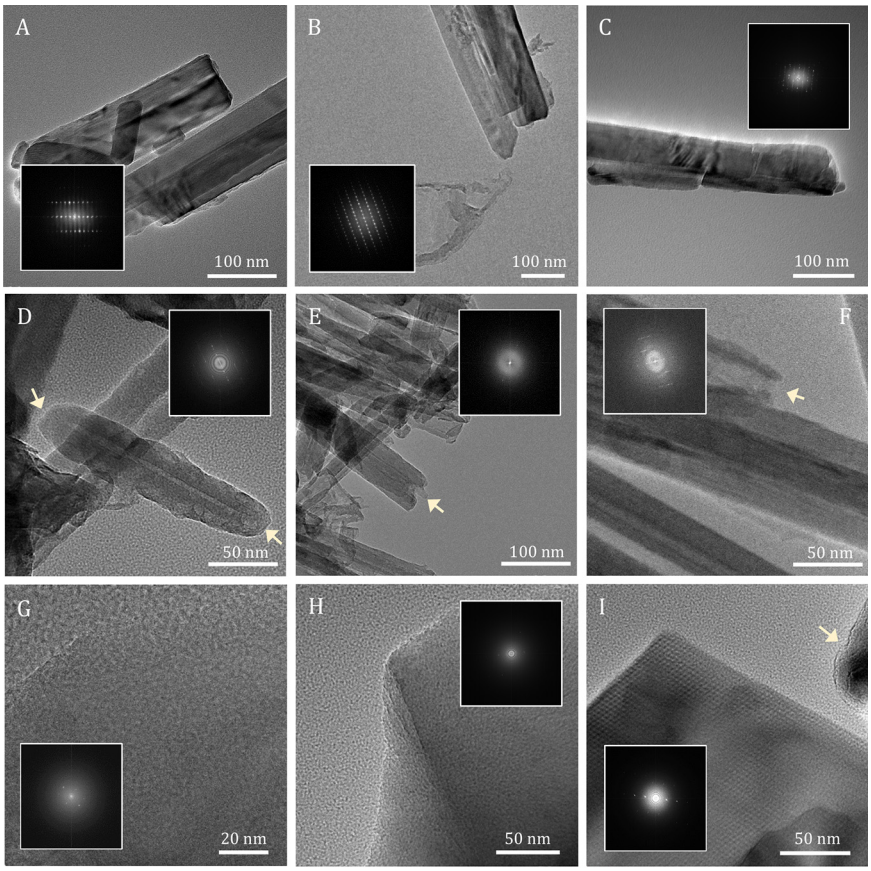

FIG 3 High-resolution scanning/transmission electron microscopy (S/TEM) and fast Fourier transform (FFT) analyses (inside S/TEM images) of crocidolite (A to C), chrysotile (D to F), and tremolite-actinolite (G to I) in the culture medium alone at 0 h (A, D, and G), incubated in the presence of microorganisms after 7 days (B, E, and H), and in the culture medium alone after 7 days (C, F, and I). The yellow arrows in panels D to F point at "closed" chrysotile particle ends at 0 h that became more "opened" after 168 h. The yellow arrow in panel I points to rounded edges in tremolite-actinolite.

(Fig. 4A; Fig. S4). Total dissolved [Si] (1.1 ± 0.06 mM) and [Mg] (1.6 ± 0.11 mM) in filtered samples from chrysotile-containing cultures matched total values (1.2 ± 0.21 mM Si and 0.87 ± 0.63 mM Mg) observed for filtered samples from chrysotile in the medium alone. Reported [Mg] values were obtained after accounting for additional dissolved [Mg] contributed by the initial *T. ammonificans* inoculum grown in the original medium, given that preinocula grown in Mg-free and Ca-free medium (used for experiments) resulted in no further growth. Corrections to dissolved [Mg] values were made for experimental cultures by subtracting the difference between initial dissolved [Mg] in chrysotile-containing medium and chrysotile-containing cultures at 0 h (0.69 ± 0.08 mM). This additional dissolved [Mg] contribution was validated in observed initial dissolved [Mg] in microbial cultures (0.72 ± 0.02 mM at 0 h) serving as positive controls under experimental conditions (Table S2). In the absence of chrysotile, filtered samples from microbial cultures resulted in total dissolved [Si] and [Mg] of 0.22 ± 0.01 mM and 0.32 ± 0.01 mM, respectively.

Tremolite-actinolite incubations resulted in overall lower total release of Si in both cultures (0.14 ± 0.02 mM) and the medium alone (0.26 ± 0.00 mM), compared to chrysotile experiments (Fig. 2B and C). In the absence of tremolite-actinolite, filtered samples from microbial cultures resulted in total dissolved [Si] of 0.11 ± 0.02 mM. Overall, total dissolved [Si] values from tremolite-actinolite incubations in the medium alone were higher than total dissolved [Si] values from cultures containing tremolite-actinolite (Fig. 2C; Fig. S3C). No evidence of biosilicification was observed in biomass produced by *T. ammonificans* in the presence of

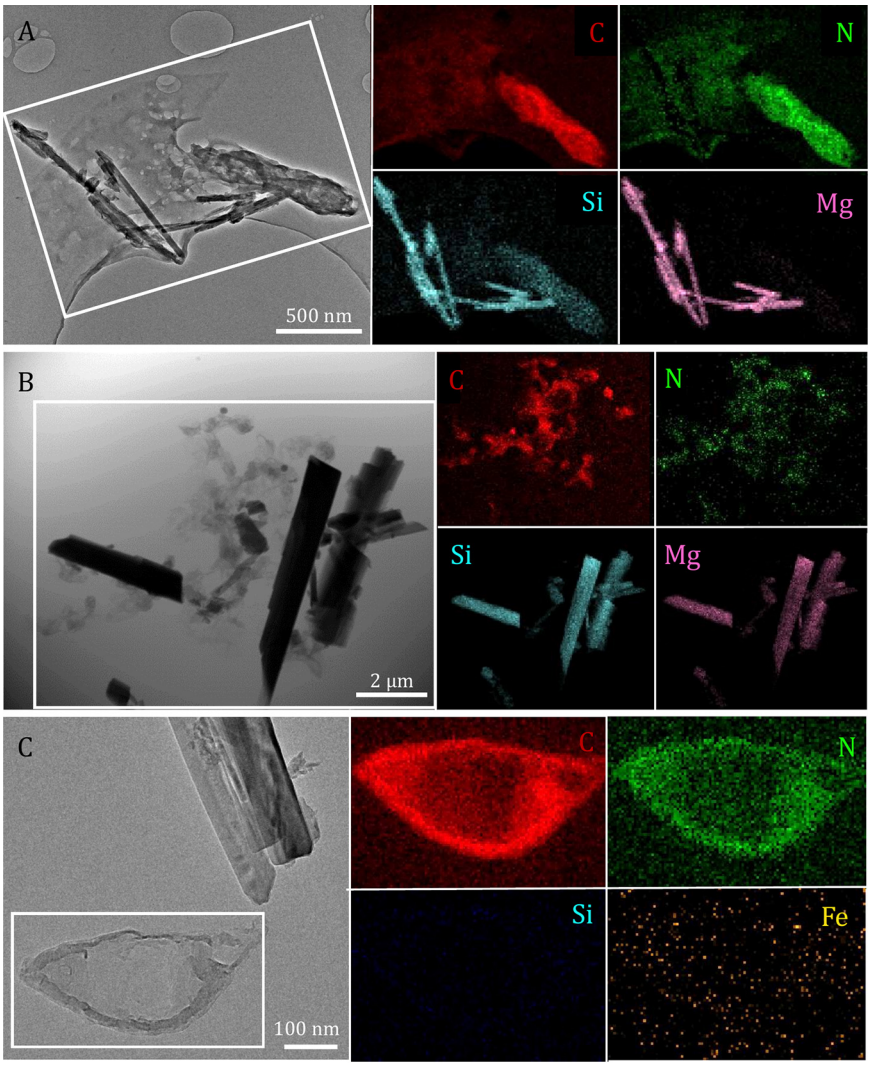

FIG 4 Scanning/transmission electron microscopy (S/TEM) images of chrysotile (A), tremolite-actinolite (B), and crocidolite (C) and their respective an energy-dispersive X-ray (EDX) spectrometer elemental mapping (of boxed areas in S/TEM images) after microbe-mineral incubations. Co-occurring maps of C (red) and N (green) were used to identify fixed microbial biomass. Maps of Si (light blue) and Mg (pink) are also shown to indicate evidence of biosilicification (when the Si map overlaps with C and N maps). Note that the S/TEM image presented in panel C is the same as in Fig. 3B, but with a different focus (in Fig. 3B we focus on the mineral and panel C we focus on the microorganism).

tremolite-actinolite (Fig. 4B). Interactions between *T. ammonificans* and tremolite-actinolite also inhibited the accumulation of dissolved [Mg] that would otherwise occur in association with tremolite-actinolite in the medium alone (Fig. 2C; Fig. S3F). Reported dissolved [Mg] values were obtained after accounting for an average of 0.71 ± 0.03 mM additional dissolved [Mg] contributed from the initial *T. ammonificans* inoculum, corrected by substracting the difference between initial dissolved [Mg] from tremolite-actinolite in the medium alone and cultures containing tremolite-actinolite. Corrected initial dissolved [Mg] values in cultures containing tremolite-actinolite are in line with documented contributions by the inoculum in chrysotile-containing experiments (which occurred under the same medium composition and temperature conditions).

Both chrysotile and tremolite-actinolite maintained the same degree of crystallinity under all experimental conditions (Fig. 3), despite chrysotile particle apices displaying signs of dissolution over time (Fig. 3D to F) and tremolite-actinolite occasionally showing particles with rounded edges (Fig. 3I). Bulk Mg/Si values of mineral particles collected from chrysotile-containing cultures averaged 1.22 ± 0.13 at 0 h, 1.16 ± 0.03 at 48 h, and

1.11 ± 0.04 at 168 h (Table S2). Bulk Mg/Si values of mineral particles collected from chrysotile-containing incubations in the medium alone averaged 1.22 ± 0.07 over the entire incubation period (Table S2). Bulk Mg/Si values of minerals collected from cultures containing tremolite-actinolite, each assumed to represent a separate microbial population (n = 3), went from 0.67 ± 0.11 at 0 h to 0.56 ± 0.03 at 48 h and to 0.56 ± 0.05 at 168 h (Table S3). Bulk Mg/Si values from tremolite-actinolite incubated in the medium alone averaged 0.56 ± 0.00 over the entire incubation period (Table S3). The original Mg/Si values for chrysotile and tremolite-actinolite have been reported to be 0.98 and 0.64, respectively (63, 64). Overall, no significant differences were observed between bulk Mg/Si values as a result of microbe-mineral interactions over time with chrysotile (1.16 ± 0.05) and tremolite-actinolite (0.59 ± 0.05) compared to bulk Mg/Si values of 1.22 ± 0.07 and 0.56 ± 0.00 resulting from chrysotile and tremolite-actinolite incubated over time in the media alone, respectively (Fig. S3A; Tables S1 and S2).

DISCUSSION

Chemolithoautotrophic Fe(III) reduction by *D. palaeochoriense* with crocidolite. Chemolithoautotrophic Fe(III) reduction activities by *D. palaeochoriense* were supported with crocidolite as the source of Fe for use as the terminal electron acceptor. Interactions between *D. palaeochoriense* and crocidolite resulted in at least ~2.2 mM Fe(II) produced [and at least ~1.95 mM Fe(III) reduced] during growth, most of which appeared to stay associated with the mineral surface (Fig. 1C). Despite the significant microbial Fe(III) reduction activities associated with crocidolite, no changes were observed in crocidolite's bulk crystallinity over time (Fig. 3A to C). Because crocidolite (like many other amphiboles) is thought to exhibit an amorphous Fe-rich coating (65–67), it is possible that microbe-mineral interactions were limited to the surface of crocidolite fibers. However, only a thin irregular layer of amorphous material (~1 to 3 nm thick [data not shown]) was occasionally detected, as partially surrounding crocidolite particles (data not shown), and no additional production of amorphous material was observed over time (Fig. 3A to C).

Alternatively, microbial reduction of structural Fe(III) in crocidolite may have been aided by a mechanism of longer-range electron transfer through electrical conductivity in the mineral's structure (68, 69). In fact, it has been proposed that the (abiotic) oxidation of Fe(II) at or above 300°C or the reduction of Fe(III) at or above 350°C in the surface of crocidolite can be maintained by migration of electrons and protons through the crystal while preserving the mineral structure (70–74). It is suggested that the initial step in the (abiotic) reduction of Fe(III) in crocidolite involves the addition of a proton (H^+) to a structural O^{2-} ion (thought to move in single jumps through structural O^{2-} ions until an OH^- ion is produced at the surface) with the simultaneous reduction of Fe(III) to Fe(II) (71, 75). Electron transfer along the silicate chain has also been proposed as a mechanism for sustained electrical conductivity in crocidolite (75). Perhaps crocidolite's bulk crystallinity in this study was maintained as a result of microbial Fe(III) reduction relying on longer-range electron transfer via the migration of electrons (and protons) through the crystal. Coupled substitutions between produced Fe(II) with dissolved Ca^{2+} or Mg^{2+} in the mineral structure (76) may also help in maintaining the crystal structure despite chemical modifications. The inhibition of Mg^{2+} release from crocidolite during microbe-mineral interactions (Fig. S2D) is consistent with the possibility of coupled substitutions in crocidolite during microbial Fe(III) reduction. Additional changes in dissolved [Si] (Fig. S3A) and in bulk Fe/Si ratios after 48 h of microbe-mineral interactions highlight co-occurring mineral alterations resulting from microbial Fe(III) reduction.

Release of Fe from crocidolite by *D. palaeochoriense* versus other biological systems. Because crocidolite—the most toxic asbestos mineral with the highest Fe content (77–80)—was the predominant commercial amphibole (81–84), treatment efforts to date have focused on removal of Fe from its surface (29, 30, 53, 85, 86). The application of Fe(III)-reducing activities by *D. palaeochoriense* in crocidolite led to significant Fe(III) reduction in the mineral (Fig. 1C) while also slightly enhancing the release of Fe

from the mineral (~0.14 mM measured by 48 h via ICP-OES). Prolonged incubation times (1 week) led to a decrease in dissolved [Fe] (Fig. 1A; Fig. S2A) and [Si] (Fig. S3A), likely due to reintroduction of Fe and Si into the mineral surface. Microbially mediated Fe release rates of ~0.006 mM Fe per gram per day were obtained from exponentially growing *D. palaeochoriense* cultures during the first 48 h of incubation. While small, these values outmatch Fe release rates from crocidolite by other biological systems studied to date (Table 1), reflecting the higher overall mobilization of Fe through the microbial respiration of Fe(III) as opposed to the trace concentration requirements for Fe during Fe assimilation.

The limited Fe removal success documented through Fe assimilation via siderophores by lichens, soil fungi, or soil bacteria (33, 53–56) reflects reduced demand for Fe via assimilation despite significant differences in biomass sizes from unicellular and microscopic to multicellular and macroscopic. Regardless, higher Fe release rates were observed for abiotic crocidolite incubations (versus biological crocidolite incubations) in saline suspensions containing sodium ascorbate at pH 7.0 and 37°C and in simulated alveolar lung fluid at pH 4.5 and 37°C (Table 1). In saline suspensions containing sodium ascorbate, ~0.82 mM dissolved [Fe] resulted from 1 g L^{-1} of crocidolite after 25 days of incubation (85). In simulated alveolar lung fluid, ~0.07 mM dissolved [Fe] resulted from 0.1 g L^{-1} of crocidolite after 90 days of incubation (86). A total of ~0.14 mM dissolved [Fe] resulted after 2 days of crocidolite incubations (10 g L^{-1}) with *D. palaeochoriense* at 60°C and pH ~6.4 in 25 mL of liquid medium (Table 1). It may be possible that sustained, steady-state Fe(III)-reducing microbial activities may generate ~0.84 mM total dissolved [Fe] (maximum dissolved [Fe] values in Table 1) after 12 days (instead of 25 days) of incubation through continuous cultivation approaches.

Substantial Fe(III) reduction activities, concurrent with enhanced Si removal from the mineral surface (~0.4 mM additional Si released by 24 h, as shown in Fig. S3A), by *D. palaeochoriense* in crocidolite may also lead to structural defects from Si loss and from the imposed changes in the oxidation state of Fe in the mineral, making it more vulnerable to downstream mechanical treatment. On the other hand, Fe redox alterations in an otherwise unchanged (and stable) crocidolite crystal structure via microbial Fe(III) reduction at 60°C may provide new access to crocidolite's properties relevant to long-range electron transfer reactions at significantly lower temperatures (60°C versus previously reported abiotic crocidolite Fe redox reactions at ≥300°C). Because Fe redox reactions in crocidolite are thought to be reversible (70–74), the potential for bidirectional electron flow within structurally unchanged mineral fibers contributes interesting properties for consideration in material science and its application. Importantly, the role of Fe redox changes associated with the reduction of Fe in crocidolite—proposed to drive mineral activation (73)—will require further research to better understand the mechanisms driving the chemical reactivity and toxicity of crocidolite asbestos.

Crystallochemical controls on biosilicification and mineral dissolution by *T. ammonificans*. Microbial biomass generated in the presence of chrysotile and ~1.1 mM dissolved [Si] displayed evidence of biosilicification (Fig. 4A). *T. ammonificans* may have also taken up ~0.12 mM Si available in the medium containing tremolite-actinolite (Fig. 2C; Fig. S3C), despite the absence of a scanning/transmission electron microscopy–energy-dispersive X-ray (S/TEM-EDX) signal for Si associated with fixed organic material (Fig. 4B). The overall lower solubility of tremolite-actinolite, which resulted in lower dissolved [Si] values than those from chrysotile, may have also contributed to an undetectable S/TEM-EDX Si signal in microbial biomass generated in the presence of tremolite-actinolite. Lower co-occurring Mg release from tremolite-actinolite (Fig. S3F) exemplifies the broad crystallochemical differences with chrysotile. Higher Si and Mg release patterns in chrysotile are consistent with the alternating Mg and Si layers in its structure, which have been shown to result in the fast initial release of Mg, followed by slower dissolution of Si-rich layers (87). Amphiboles such as tremolite-actinolite, on the other hand, have been shown to dissolve less quickly than chrysotile due to the formation of an amorphous outer layer rich in Fe species (88, 89). While the bulk crystallinity

TABLE 1 Compiled Fe release rates from UICC crocidolite during different chemical and biological treatments[a]

Reference	Organism/medium	Temp (°C)	Initial pH	Starting asbestos amt (g L^{-1})	Incubation time (days)	Initial $[Fe]_{aq}$ (mM)	Final $[Fe]_{aq}$ (mM)	Fe release rate (mM g^{-1} day^{-1})
85	Saline suspension + sodium ascorbate	37	7	1.0 (reported as 1 mg/mL in a total of 250 mL)	25	0*	0.82 (reported as 820 μmol/g in Table 1 of the reference)	0.03
86	Simulated alveolar lung fluid	37	4.5	0.1 (reported as 0.025 g in 250 mL)	90	0	0.072 (reported as ~4,000 ppb)	0.008
This study	*D. palaeochoriense*/modified DSM 1210	60	6.4	10.0	2	0.03	0.14	0.006
29	*F. oxysporum*/Czapek	25	5.5	2.1 (reported as 50 mL of 0.023g/mL added to 500 mL cultures)	56	0.03	0.35 (reported in Fig. 2 of the reference)	0.003
30	*Verticillium* spp./Czapek	25	5.5	23.0	20	0*	0.81	0.002
53	*Mortierella hyalina*/Czapek	25	5.5	2.0	45	0	0.2 (reported as nmol Fe/mg crocidolite in Fig. 5 of the reference)	0.002
85	Saline suspension	37	7	1.0	25	0*	0.023	0.0009
53	*Fusarium oxysporum*/Czapek	25	5.5	2.0	45	0	0.04 (reported as nmol Fe/mg crocidolite in Fig. 5 of the reference)	0.0004
30	*F. oxysporum*/Czapek	25	5.5	23.0	20	0*	0.12	0.0003
30	*Paecilomyces* spp./Czapek	25	5.5	23.0	20	0*	0.11	0.0003

[a]Data are organized by decreasing Fe release rates. Compiled Fe release rates are expressed as millimolar concentrations per gram of crocidolite initially provided per day. Initial dissolved [Fe] values marked with an asterisk are assumed values, as data are not available from the reference. Data obtained in this study and values for Fe release rates are shaded.

in both chrysotile and tremolite-actinolite was maintained over time (Fig. 3), the evidence of surficial dissolution at particle apices of chrysotile also reflects the higher overall Si and Mg release observed in chrysotile (Fig. 3D to F). Some minor evidence of dissolution in tremolite-actinolite was observed in the form of rounded particle edges (Fig. 3I) and through the presence of some amorphous surfaces (data not shown).

Dissolution differences between chrysotile and tremolite-actinolite were also observed for Fe, Al, and Ca (Fig. S9). Microbial inhibition of the release of Fe that would otherwise occur during chrysotile incubations in the medium alone highlight possible Fe uptake and assimilation activities by *T. ammonificans* during growth (Fig. S9B). The overall release of Fe from chrysotile incubations in the medium alone is also relevant to the removal of Fe from the mineral (Fig. S9B). No significant changes in Fe release resulted from microbial cultures with tremolite-actinolite (Fig. S9C), which instead led to the inhibition of Ca and Al release that would otherwise occur during tremolite-actinolite incubations in the medium alone (Fig. S9F and I). Crystallochemical properties not only are likely to drive resulting elemental dissolution patterns but also appear to dictate the bioavailability of elements relevant to *T. ammonificans* microbial growth.

Biologically mediated release of Si and Mg from chrysotile. Because chrysotile is, by far, the predominant commercial form of asbestos, the release of Si and Mg from its magnesium silicate framework has been a focus of study involving its dissolution (36, 90, 91). While the presence of *T. ammonificans* did not enhance Mg and Si leaching from chrysotile, overall Si and Mg release rates observed in our experimental incubations (Table 2) outmatched Si and Mg release rates obtained from biologically mediated chrysotile dissolution studies using a fungal system (36). Si release rates comparable to the ones reported in this study ($\sim$0.5 mM g^{-1} day^{-1}) were obtained from chrysotile incubations in water ($\sim$0.4 mM g^{-1} day^{-1}) at pH 4.0 and 25°C under anoxic ("CO_2-free nitrogen") conditions (90). Lower Mg release rates ($\sim$0.6 mM g^{-1} day^{-1}) cooccurred with Si release rates in our study in comparison to Mg release rates for chrysotile incubations ($\sim$1.1 mM Si g^{-1} day^{-1}) in water (90). Under anoxic conditions at pH 4.0 and 25°C, $\sim$1.4 mM dissolved [Si] and $\sim$3.9 mM dissolved [Mg] resulted from 0.5 g L^{-1} of chrysotile after $\sim$7 days of incubation (90). Because a total of $\sim$1.1 mM dissolved [Si] and $\sim$1.8 mM dissolved [Mg] resulted after 2 days of chrysotile incubations (1 g L^{-1}) at 75°C and pH 5.5 (Table 2), it may be possible that sustained, steady-state incubations may generate $\sim$3.8 mM total dissolved [Si] and $\sim$6.3 mM total dissolved [Mg] after 1 week under chemostatic conditions.

Conclusions. Interactions between *D. palaeochoriense* and crocidolite illustrate the capability of microbial Fe(III) reduction to substantially change the oxidation state of Fe within the amphibole mineral while also contributing, albeit to a lesser extent, to the release of Fe from its surface—without altering the mineral structure. This removal of Fe from crocidolite through respiratory Fe(III) reduction outperforms Fe assimilation as a biological mechanism for the removal of Fe from crocidolite. Interactions between *T. ammonificans* and chrysotile or tremolite-actinolite highlight the relevance behind the crystallochemical differences among serpentine (chrysotile) and amphibole (tremolite-actinolite) asbestos in controlling mineral-processing effectiveness and elemental bioavailability. Despite the lack of microbially mediated Si and Mg release of chrysotile by *T. ammonificans* (which displayed evidence of biosilicification), experimental conditions in our study outmatched previously reported Si and Mg release rates during chrysotile dissolution by fungi. Additional constraints on the relationships between elemental release rates, amount of starting asbestos, reaction volumes, and incubation times will be required to better compare the performance of biological and abiotic asbestos dissolution treatments studied to date.

MATERIALS AND METHODS

Microbe-mineral experiments, mineral preparation, and culture conditions. Chemolithoautotrophic Fe(III) reduction by *Deferrisoma palaeochoriense* (61) was tested for the removal of Fe from crocidolite (62), an amphibole asbestos containing about $\sim$38 wt % (where wt % means weight percent) Fe oxides (versus 3 to 5 wt % Fe oxides in chrysotile and tremolite-actinolite, the other minerals used in this study, as shown in Table S4). Reference crocidolite from the Union for International Cancer Control (UICC) was

TABLE 2 Compiled Si and Mg release rates from chrysotile asbestos during different chemical and biological treatments[a]

Reference	Organism/medium	Temp (°C)	Initial pH	Mineral	Starting asbestos amt (g L^{-1})	Incubation time (days)	Initial $[Si]_{aq}$ (mM)	Final $[Si]_{aq}$ (mM)	Si release rate (mM g^{-1} day^{-1})	Initial $[Mg]_{aq}$ (mM)	Final $[Mg]_{aq}$ (mM)	Mg release rate (mM g^{-1} day^{-1})
This study	*T. ammonificans*/modified SME	75	5.5	Chrysotile (Balangero, Italy)	1.0	2	0.21	1.10	0.45	0.55	1.83	0.64
90	Water	25	4	Chrysotile (Thetford, Canada)	0.5	7.1	0*	1.4	0.40	0*	3.94	1.1
36	*Verticillium leptobactrum*/Czapek	25	5.5	Chrysotile (Balangero, Italy)	2.3	20	0*	1.9	0.04	0*	4.7	0.10
91	Sulfuric acid (0.05 M) (used highest values in Table 3 of the reference)	25	1.3	Chrysotile (Málaga, Spain)	2.0	30	0*	1.9	0.03	0*	22	0.37
91	Oxalic acid (0.2 M) (used highest values in Table 4 of the reference)	25	1.2	Chrysotile (Málaga, Spain)	2.0	30	0*	1.2	0.02	0*	21	0.35
91	Nitric acid (0.1 M) (used highest values in Table 2 of the reference)	25	1.2	Chrysotile (Málaga, Spain)	2.0	30	0*	1.4	0.02	0*	17	0.28
90	Water	25	9	Chrysotile (Thetford, Canada)	0.5	7.1	0*	0.044	0.01	0*	0.18	0.05
36	*Fusarium oxysporum*/Czapek	25	5.5	Chrysotile (Balangero, Italy)	2.3	20	0*	0.3	0.007	0*	2.4	0.05
90	Water	25	7	Chrysotile (Thetford, Canada)	0.5	43	0*	0.1	0.005	0*	0.42	0.02

[a]Data are organized by decreasing Si release rates. Si and Mg release rates are provided as millimolar concentrations per gram of chrysotile initially provided per day. Initial dissolved [Si] and [Mg] marked with an asterisk are assumed values, as data are not available from the reference. Note that chrysotile incubations in modified SME medium in the absence of *T. ammonificans* yielded Si and Mg release rates similar to those reported in this table. Data obtained in this study and values for Si and Mg release rates are shaded.

used as obtained at a final concentration of 10 g L^{-1}, which equaled ~10 mM Fe(III) [the smallest amount of Fe(III) provided that supported the production of known maximal cell concentrations after incubation (Fig. S5A)]. Microbe-mineral experiments with *D. palaeochoriense* were performed under optimal growth conditions (60°C, pH 6.1 to 6.4, 1.5 wt % NaCl) using a Mg- and Ca-modified version (see supporting information) of the modified (61) DSM 1210 medium (92). Modifications in the content of Mg and Ca in the medium were performed to better monitor aqueous Mg and Ca changes associated with microbe-mineral interactions. The selected Mg and Ca medium modifications did not affect *D. palaeochoriense*'s growth (Fig. S5B). Anaerobic cultivation in sterilized (autoclaved) media included a gas phase of H_2/CO_2 (80%:20% [vol/vol], 0.2 MPa), with H_2 as the primary electron donor, CO_2 as the C source, and ~10 mM Fe(III)—from poorly crystalline $Fe(OH)_3$ in the positive control or crocidolite in experimental assays—as the terminal electron acceptor.

Bacterial biosilicification (Fig. S6) by *Thermovibrio ammonificans* (93) was tested for the removal Si and Mg from serpentine (chrysotile) and amphibole (tremolite-actinolite) asbestos (Table S4). Chrysotile [crystal-chemical formula: $(Mg_{5.81}Fe^{2+}_{0.15}A_{l0.27}Fe^{3+}_{0.09}Cr_{0.01})_{6.33}Si_{3.97}O_{10}(OH)_{7.11}$ (63)] and tremolite-actinolite [crystal-chemical formula: $(Na_{0.07}\ K_{0.01})(Ca_{1.96}\ Mn_{0.02}\ Fe^{2+}_{0.02})(Mg_{4.41}\ Fe^{2+}_{0.58}\ Mn_{0.01}\ Al_{0.01})(Si_{7.92}\ Al_{0.07})(OH_{1.98}\ F_{0.02})$ (64)] mineral samples were purified, ground, and filtered, while preserving the original aspect ratio (94). Subsequently, particles were sterilized and suspended in water under an N_2 (100% [vol/vol], 0.2 MPa) gas phase (94). The final concentration of these two minerals in microbial cultures was 1 g L^{-1} as the lowest concentration possible without affecting microbial growth (Fig. S7). Microbe-mineral experiments with *T. ammonificans* were performed under optimal growth conditions (75°C, pH 5.5, 2 wt % NaCl) using a Mg- and Ca-free version (Fig. S8) of the modified (93) SME medium (95). Anaerobic cultivation conditions included a gas phase of H_2 and CO_2 (80%:20% [vol/vol], 0.2 MPa), with H_2 as the primary electron donor, CO_2 as the C source, and KNO_3 (~20 mM) as the terminal electron acceptor. The absence of initial organic compounds in the media used for chemolithoautotrophic growth in our microbe-mineral experiments helped us to identify asbestos interactions with organic substrates (96) as the result of microbial growth via CO_2 fixation.

All microbe-mineral experiments were carried out in 25 mL of media in serum bottles for 1 week in triplicate, together with triplicate positive controls of microorganisms grown in the absence of minerals and triplicate negative controls of the minerals in media alone. Samples for direct cell counts (7 or 8 per culture), aqueous chemical analysis (7 or 8 per serum bottle), and mineralogical characterization (3 per serum bottle with asbestos) were collected periodically over time to characterize potential mineral dissolution as a result of microbial growth.

Measurements of cell concentrations and aqueous chemistry. Microbial growth was documented via direct cell counts of culture samples (0.25 to 0.5 mL) fixed with 25 μL of 25% (vol/vol) glutaraldehyde and stained with 0.1% (wt/vol) acridine orange. Stained cells filtered onto a 0.2-μm-pore-size black polycarbonate filter were visualized under an Olympus BX53 microscope with a 100× oil immersion objective (UPlanF1 100/1.3) and X-Cite 120 light-emitting diode (LED) fluorescence lamp. Cell concentration estimates (in cells per milliliter) were obtained from cell counts performed in 10 separate 50- by 50-μm grid areas of microscopy images taken with a digital camera system using the image analysis software CellSens Dimension. Calculations associated with cell concentrations and cell doubling times are described in the supplemental material.

Aqueous concentrations of Si, Mg, Ca, Al, and Fe were determined using a ICP-OES equipped with a modified Lichte nebulizer and 25-mm axial plasma torch. Briefly, culture samples (1.0 mL) were centrifuged for at least 5 min at 10,000 × *g* immediately after collection and the supernatant was subsequently filtered through a 0.2-μm-pore-size syringe filter. Aqueous [Si], [Mg], [Ca], [Al], and [Fe] were determined from filtrates (stored at −20°C until analysis) at wavelengths of 251 nm, 288 nm, 315 nm, 308 nm, and 259 nm, respectively. All reported aqueous elemental concentrations obtained via ICP-OES were generated by subtracting values of negative-control measurements from values of experimental measurements.

Additional [Fe(II)] and [Fe(III)] measurements were obtained from crocidolite experiments and Fe$(OH)_3$-containing controls (for positive microbial growth through chemolithoautotrophic Fe(III) reduction) using a modification (97) of the ferrozine assay (98). Filtrate samples (0.5 mL) generated as described above were acidified using 2 N HCl to prevent abiotic Fe(II) oxidation and stored at −20°C until analysis. Spectrophotometric measurements of both aqueous [Fe(II)] and [Fe(III)] were performed on acidified filtrates diluted with 0.5 N HCl for a total volume of 0.2 mL using a SpectraMax Plus 384 spectrophotometer at 562 nm. Total extractable [Fe(II)] and [Fe(III)] from crocidolite and $Fe(OH)_3$ were also obtained from unfiltered culture samples (0.5 mL) digested for 8 h (Fig. S9) in 12 N HCl (1:1 ratio) before 0.5 N HCl dilutions for the ferrozine assay as described above. Obtained values of total extractable [Fe(II)] and [Fe(III)] for each individual sample were added to obtain the total extractable [Fe], and this total value was used to normalize changes of total extractable [Fe(II)] and [Fe(III)] within each time series. For more details on [Fe(II)] and [Fe(III)] measurements in unfiltered culture samples, please see the supplemental material.

Electron microscopy. Mineral particles collected after centrifugation of samples taken for chemical analysis at 0 h and 48 h and after 1 week were resuspended twice in clean Milli-Q water and centrifuged again, and the overlaying water was discarded to remove salts originating from culture media. Subsequently, the mineral samples were air dried and stored at room temperature before being transferred onto 12-mm carbon tabs (Pelco) for electron microscopy. The mineral samples were analyzed using a FEI Quanta 600 FEG Mark II environmental scanning electron microscope (ESEM) equipped with an energy-dispersive X-ray (EDX) spectrometer. The instrument was used in environmental mode, with a voltage of 15 kV and a chamber pressure of 0.53 torr. Variable-spot dimensions were used to optimize imaging or chemical analysis. For all samples, 25 EDX spot analyses were performed, spread across 5

areas (5 spot analyses per area) at a fixed magnification of ×5,000. Averaged bulk elemental compositions (atomic percent) of mineral samples, determined from the EDX spot analyses, were used to calculate Mg/Si or Fe/Si values. Reported bulk compositions included the surface and near-surface areas of the minerals.

Scanning/transmission electron microscopy (S/TEM) analyses were also performed on air-dried mineral samples transferred onto 300-mesh lacey-carbon copper grids leaning on a mixed cellulose ester filter. Grids were investigated with a JEOL-F200 multipurpose analytical S/TEM (equipped with a cold-field emission gun and two large-area EDX spectrometers) operated at 200 kV. High-resolution S/TEM imaging in combination with fast Fourier transform (FFT) image elaboration was used to determine the degree of mineral crystallinity, and S/TEM-EDX mapping was performed to detect, characterize, and define the spatial location of biomass in relation to the mineral particles. The effects of the S/TEM electron beam and of the culture media on mineral stability were also taken into consideration as part of these analyses (Fig. S10 and S11).

SUPPLEMENTAL MATERIAL

Supplemental material is available online only.

SUPPLEMENTAL FILE 1, PDF file, 5.5 MB.

ACKNOWLEDGMENTS

We thank David Vann in the Department of Earth and Environmental Science, University of Pennsylvania (Penn), for his help in conducting ICP-OES analyses and for his many constructive discussions regarding asbestos. We also thank Sabrina Elkassas and Kenneth Cho for their assistance with medium preparation.

This research was supported by Penn Start-up Funds and Elliman Faculty Fellowship to I.P.-R. as well as grants P30-ES013508 and P42-ES023720 from the National Institute of Environmental Health Sciences (NIEHS) of the National Institutes of Health (NIH). The contents are solely the responsibility of the authors and do not necessarily represent the official views of NIEHS and NIH. Part of this work was carried out at the Singh Center for Nanotechnology, part of the National Nanotechnology Coordinated Infrastructure Program, which is supported by National Science Foundation (NSF) grant NNCI-1542153.

REFERENCES

1. Virta RL. 2002. Asbestos: geology, mineralogy, mining, and uses, p 1–28. *In* USGS open-file report 02-149. US Department of the Interior, US Geological Survey, Reston, VA.
2. Murray R. 1990. Asbestos: a chronology of its origins and health effects. Br J Ind Med 47:361–365. https://doi.org/10.1136/oem.47.6.361.
3. Alleman JE, Mossman BT. 1997. Asbestos revisited. Sci Am 277:70–75. https://doi.org/10.1038/scientificamerican0797-70.
4. Virta RL. 2005. Mineral commodity profiles—asbestos, p 1–56. *In* USGS circular 1255-KK. US Department of the Interior, US Geological Survey, Reston, VA.
5. Ross M, Langer AM, Nord GL, Nolan RP, Lee RJ, Van Orden D, Addison J. 2008. The mineral nature of asbestos. Regul Toxicol Pharmacol 52:S26–S30. https://doi.org/10.1016/j.yrtph.2007.09.008.
6. Bégin R, Cantin A, Massé S. 1989. Recent advances in the pathogenesis and clinical assessment of mineral dust pneumoconiosis: asbestosis, silicosis and coal pneumoconiosis. Eur Respir J 2:988–1001. https://doi.org/10.1183/09031936.93.02100988.
7. Mossman BT, Bignon J, Corn M, Seaton A, Gee JBL. 1990. Asbestos: scientific developments and implications for public policy. Science 247:294–301. https://doi.org/10.1126/science.2153315.
8. Doll NJ, Stankus RP, Barkman HW. 1983. Immunopathogenesis of asbestosis, silicosis, and coal workers' pneumoconiosis. Clin Chest Med 4:3–14. https://doi.org/10.1016/S0272-5231(21)00179-9.
9. Mossman BT, Churg A. 1998. Mechanisms in the pathogenesis of asbestosis and silicosis. Am J Respir Crit Care Med 157:1666–1680. https://doi.org/10.1164/ajrccm.157.5.9707141.
10. Wagner JC, Sleggs CA, Marchand P. 1960. Diffuse pleural mesothelioma and asbestos exposure in the north western Cape Province. Br J Ind Med 17:260–271. https://doi.org/10.1136/oem.17.4.260.
11. Weitzman SA, Weitberg AB. 1985. Asbestos-catalyzed lipid peroxidation and its inhibition by desferroxamine. Biochem J 225:259–262. https://doi.org/10.1042/bj2250259.
12. Goodlick LA, Kane AB. 1986. Role of reactive oxygen metabolites in crocidolite asbestos toxicity to mouse macrophages. Cancer Res 46:5558–5566.
13. Mossman BT, Marsh JP, Shatos MA. 1986. Alteration of superoxide dismutase activity in tracheal epithelial cells by asbestos and inhibition of cytotoxicity by antioxidants. Lab Invest 54:204–212.
14. Shatos MA, Doherty JM, Marsh JP, Mossman BT. 1987. Prevention of asbestos induced cell death in rat lung fibroblasts and alveolar macrophages by scavengers of active oxygen species. Environ Res 44:103–116. https://doi.org/10.1016/s0013-9351(87)80090-7.
15. Kamp DW, Graceffa P, Pryor WA, Weitzman SA. 1992. The role of free radicals in asbestos-induced diseases. Free Radic Biol Med 12:293–315. https://doi.org/10.1016/0891-5849(92)90117-y.
16. Mossman BT, Marsh JP. 1989. Evidence supporting a role for active oxygen species in asbestos-induced toxicity and lung disease. Environ Health Perspect 81:91–94. https://doi.org/10.1289/ehp.898191.
17. Fubini B, Mollo L. 1995. Role of iron in the reactivity of mineral fibers. Toxicol Lett 82–83:951–960. https://doi.org/10.1016/0378-4274(95)03531-1.
18. Fubini B, Otero Areán C. 1999. Chemical aspects of the toxicity of inhaled mineral dusts. Chem Soc Rev 28:373–381. https://doi.org/10.1039/a805639k.
19. Mossman BT, Borm PJ, Castranova V, Costa DL, Donaldson K, Kleeberger SR. 2007. Mechanisms of action of inhaled fibers, particles and nanoparticles in lung and cardiovascular diseases. Part Fibre Toxicol 4:4. https://doi.org/10.1186/1743-8977-4-4.
20. Aust AE, Cook PM, Dodson RF. 2011. Morphological and chemical mechanisms of elongated mineral particle toxicities. J Toxicol Environ Health B Crit Rev 14:40–75. https://doi.org/10.1080/10937404.2011.556046.
21. Selikoff IJ, Churg J, Hammond EC. 1965. Relation between exposure to asbestos and mesothelioma. N Engl J Med 272:560–565. https://doi.org/10.1056/NEJM196503182721104.
22. Middleton AP, Beckett ST, Davis JMG. 1979. Further observations on the short-term retention and clearance of asbestos by rates, using UICC reference samples. Ann Occup Hyg 22:141–152.
23. Ohlson CG, Hogstedt C. 1985. Lung cancer among asbestos cement workers. A Swedish cohort study and a review. Br J Ind Med 42:397–402. https://doi.org/10.1136/oem.42.6.397.

24. Langer AM, Nolan RP. 1989. Fibre type and burden in parenchymal tissues of workers occupationally exposed to asbestos in the United States. IARC Sci Publ 90:330–335.
25. Skinner HCW. 2003. Mineralogy of asbestos minerals. Indoor Built Environ 12:385–389. https://doi.org/10.1177/1420326X03037003.
26. Berman DW, Crump KS. 2008. A meta-analysis of asbestos-related cancer risk that addresses fiber size and mineral type. Crit Rev Toxicol 38:49–73. https://doi.org/10.1080/10408440802273156.
27. Berman DW, Crump KS, Chatfield EJ, Davis JMG, Jones AD. 1995. The sizes, shapes, and mineralogy of asbestos structures that induce lung tumors or mesothelioma in AF/HAN rats following inhalation. Risk Anal 15:181–195. https://doi.org/10.1111/j.1539-6924.1995.tb00312.x.
28. Tomatis M, Turci F, Ceschino R, Riganti C, Gazzano E, Martra G, Ghigo D, Fubini B. 2010. High aspect ratio materials: role of surface chemistry vs. length in historical long and short amosite asbestos fibers. Inhal Toxicol 22:984–998. https://doi.org/10.3109/08958378.2010.504243.
29. Daghino S, Martino E, Fenoglio I, Tomatis M, Perotto S, Fubini B. 2005. Inorganic materials and living organisms: surface modifications and fungal responses to various asbestos forms. Chemistry 11:5611–5618. https://doi.org/10.1002/chem.200500046.
30. Daghino S, Turci F, Tomatis M, Favier A, Perotto S, Douki T, Fubini B. 2006. Soil fungi reduce the iron content and the DNA damaging effects of asbestos fibers. Environ Sci Technol 40:5793–5798. https://doi.org/10.1021/es060881v.
31. Favero-Longo SE, Turci F, Fubini B, Castelli D, Piervittori R. 2013. Lichen deterioration of asbestos and asbestiform minerals of serpentinite rocks in Western Alps. Int Biodeterior Biodegradation 84:342–350. https://doi.org/10.1016/j.ibiod.2012.07.018.
32. Salamatipour A, Mohanty SK, Pietrofesa RA, Vann DR, Christofidou-Solomidou M, Willenbring JK. 2016. Asbestos fiber preparation methods affect fiber toxicity. Environ Sci Technol Lett 3:270–274. https://doi.org/10.1021/acs.estlett.6b00174.
33. Mohanty SK, Gonneau C, Salamatipour A, Pietrofesa RA, Casper B, Christofidou-Solomidou M, Willenbring JK. 2018. Siderophore-mediated iron removal from chrysotile: implications for asbestos toxicity reduction and bioremediation. J Haz Mater 341:290–296. https://doi.org/10.1016/j.jhazmat.2017.07.033.
34. Favero-Longo SE, Turci F, Tomatis M, Castelli D, Bonfante P, Hochella MF, Piervittori R, Fubini B. 2005. Chrysotile asbestos is progressively converted into a non-fibrous amorphous material by the chelating action of lichen metabolites. J Environ Monit 7:764–766. https://doi.org/10.1039/b507569f.
35. Turci F, Favero-Longo SE, Tomatis M, Martra G, Castelli D, Piervittori R, Fubini B. 2007. A biomimetic approach to the chemical inactivation of chrysotile fibres by lichen metabolites. Chem Eur J 13:4081–4093. https://doi.org/10.1002/chem.200600991.
36. Daghino S, Turci F, Tomatis M, Girlanda M, Fubini B, Perotto S. 2009. Weathering of chrysotile asbestos by the serpentine rock-inhabiting fungus Verticillium leptobactrum. FEMS Microbiol Ecol 69:132–141. https://doi.org/10.1111/j.1574-6941.2009.00695.x.
37. Valouma A, Verganelaki A, Maravelaki-Kalaitzaki P, Gidarakos E. 2016. Chrysotile asbestos detoxification with a combined treatment of oxalic acid and silicates producing amorphous silica and biomaterial. J Haz Mater 305:164–170. https://doi.org/10.1016/j.jhazmat.2015.11.036.
38. Sugama T, Sabatini R, Petrakis L. 1998. Decomposition of chrysotile asbestos by fluorosulfonic acid. Ind Eng Chem Res 37:79–88. https://doi.org/10.1021/ie9702744.
39. Plescia P, Gizzi D, Benedetti S, Camilucci L, Fanizza C, De Simone P, Paglietti F. 2003. Mechanochemical treatment to recycling asbestos-containing waste. Waste Manag 23:209–218. https://doi.org/10.1016/S0956-053X(02)00156-3.
40. Anastasiadou K, Axiotis D, Gidarakos E. 2010. Hydrothermal conversion of chrysotile asbestos using near supercritical conditions. J Haz Mater 179:926–932. https://doi.org/10.1016/j.jhazmat.2010.03.094.
41. Kusiorowski R, Zaremba T, Piotrowski J, Gerle A. 2013. Thermal decomposition of asbestos-containing materials. J Therm Anal Calorim 113:179–188. https://doi.org/10.1007/s10973-013-3038-y.
42. Zhai W, Wang Y, Deng Y, Gao H, Lin Z, Li M. 2014. Recycling of asbestos tailings used as reinforcing fillers in polypropylene-based composites. J Haz Mater 270:137–143. https://doi.org/10.1016/j.jhazmat.2014.01.052.
43. Granat K, Nowak D, Pigiel M, Florczak W, Opyd B. 2015. Application of microwave radiation in innovative process of neutralising asbestos-containing wastes. Arch Civ Mech Eng 15:188–194. https://doi.org/10.1016/j.acme.2014.05.012.
44. Tabata M, Shono A, Ghaffar A. 2016. Decomposition of asbestos by a supernatant used for immobilization of heavy metals in fly ash. J Mater Cycles Waste Manag 18:483–492. https://doi.org/10.1007/s10163-016-0491-2.
45. Ruiz AI, Ortega A, Fernández R, Miranda JF, López SE, Cuevas J. 2018. Thermal treatment of asbestos containing materials (ACM) by mixing with Na_2CO_3 and special clays for partial vitrification of waste. Mater Lett 232:29–32. https://doi.org/10.1016/j.matlet.2018.08.061.
46. Pacella A, Tomatis M, Viti C, Bloise A, Arrizza L, Ballirano P, Turci F. 2020. Thermal inertization of amphibole asbestos modulates Fe topochemistry and surface reactivity. J Haz Mater 398:123119. https://doi.org/10.1016/j.jhazmat.2020.123119.
47. Hong MH, Joo SY, Kim S, Lee CG, Kim DW, Yoon J-H. 2020. Asbestos-containing waste detoxification by a microwave heat treatment using silicon carbide as an inorganic heating element. J Mater Cycles Waste Manag 22:826–835. https://doi.org/10.1007/s10163-020-00977-9.
48. Marian NM, Giorgetti G, Magrini C, Capitani GC, Galimberti L, Cavallo A, Salvini R, Vanneschi C, Viti C. 2021. From hazardous asbestos containing wastes (ACW) to new secondary raw material through a new sustainable inertization process: a multimethodological mineralogical study. J Haz Mater 413:125419. https://doi.org/10.1016/j.jhazmat.2021.125419.
49. Crawford RH, Floyd M, Li CY. 2000. Degradation of serpentine and muscovite rock minerals and immobilization of cations by soil Penicillium spp. Phyton 40:315–321.
50. Martino E, Cerminara S, Prandi L, Fubini B, Perotto S. 2004. Physical and biochemical interactions of soil fungi with asbestos fibers. Environ Toxicol Chem 23:938–944. https://doi.org/10.1897/03-266.
51. Favero-Longo SE, Siniscalco C, Piervittori R. 2006. Plant and lichen colonization in an asbestos mine: spontaneous bioattenuation limits air dispersion of fibres. Plant Biosyst 140:190–205. https://doi.org/10.1080/11263500600756546.
52. Wallis SL, Emmett EA, Hardy R, Casper BB, Blanchon DJ, Testa JR, Menges CW, Gonneau C, Jerolmack DJ, Seiphoori A, Steinhorn G, Berry T-A. 2020. Challenging global waste management—bioremediation to detoxify asbestos. Front Environ Sci 8:20. https://doi.org/10.3389/fenvs.2020.00020.
53. Martino E, Prandi L, Fenoglio I, Bonfante P, Perotto S, Fubini B. 2003. Soil fungal hyphae bind and attack asbestos fibers. Angew Chem Int Ed Engl 42:219–222. https://doi.org/10.1002/anie.200390083.
54. Stanik IA, Cedzyńska K, Żakowska Z. 2006. Destruction of the chrysotile asbestos structure with a population of bacteria Lactobacillus casei and Lactobacillus plantarum. Fresenius Environ Bull 15:640–643.
55. Daghino S, Martino E, Vurro E, Tomatis M, Girlanda M, Fubini B, Perotto S. 2008. Bioweathering of chrysotile by fungi isolated in ophiolitic sites. FEMS Microbiol Lett 285:242–249. https://doi.org/10.1111/j.1574-6968.2008.01239.x.
56. Bhattacharya S, John PJ, Ledwani L. 2016. Fungal weathering of asbestos is semi arid regions of India. Ecotoxicol Environ Saf 124:186–192. https://doi.org/10.1016/j.ecoenv.2015.10.022.
57. Spiess FN, Macdonald KC, Atwater T, Ballard R, Carranza A, Cordoba D, Cox C, Garcia VM, Francheteau J, Guerrero J, Hawkins J, Haymon R, Hessler R, Juteau T, Kastner M, Larson R, Luyendyk B, Macdougall JD, Miller S, Normark W, Orcutt J, Rangin C. 1980. East Pacific Rise: hot springs and geophysical experiments. Science 207:1421–1433. https://doi.org/10.1126/science.207.4438.1421.
58. Karageorgis A, Anagnostou C, Sioulas A, Chronis G, Papathanassiou E. 1998. Sediment geochemistry and mineralogy in Milos bay, SW Kyklades, Aegean Sea, Greece. J Mar Syst 16:269–281. https://doi.org/10.1016/S0924-7963(97)00020-1.
59. Lalonde SV, Konhauser KO, Reysenbach A-L, Ferris FG. 2005. The experimental silicification of Aquificales and their role in hot spring sinter formation. Geobiology 3:41–52. https://doi.org/10.1111/j.1472-4669.2005.00042.x.
60. Ikeda T. 2021. Bacterial biosilicification: a new insight into the global silicon cycle. Biosci Biotechnol Biochem 85:1324–1331. https://doi.org/10.1093/bbb/zbab069.
61. Pérez-Rodríguez I, Rawls M, Coykendall DK, Foustoukos DI. 2016. Deferrisoma palaeochoriense sp. nov., a thermophilic, iron(III)-reducing bacterium from a shallow-water hydrothermal vent in the Mediterranean Sea. Int J Syst Evol Microbiol 66:830–836. https://doi.org/10.1099/ijsem.0.000798.
62. Bowes DR, Farrow CM. 1997. Major and trace element compositions of the UICC standard asbestos samples. Am J Ind Med 32:592–594. https://doi.org/10.1002/(SICI)1097-0274(199712)32:6%3C592::AID-AJIM3%3E3.0.CO;2-S.
63. Pollastri S, Perchiazzi N, Lezzerini M, Plaisier JR, Cavallo A, Dalconi MC, Gandolfi NB, Gualtieri AF. 2016. The crystal structure of mineral fibres: 1. Chrysotile. Period Mineral 85:249–259.

64. Vigliaturo R, Della Ventura G, Choi JK, Marengo A, Lucci F, O'Shea MJ, Pérez-Rodríguez I, Gieré R. 2018. Mineralogical characterization and dissolution experiments in Gamble's solution of tremolitic amphibole from Passo di Caldenno (Sondrio, Italy). Minerals 8:557. https://doi.org/10.3390/min8120557.
65. Fantauzzi M, Pacella A, Atzei D, Gianfagna A, Andreozzi GB, Rossi A. 2010. Combined use of X-ray photoelectron and Mössbauer spectroscopic techniques in the analytical characterization of iron oxidation state in amphibole asbestos. Anal Bioanal Chem 396:2889–2898. https://doi.org/10.1007/s00216-010-3576-0.
66. Vigliaturo R, Pollastri S, Gieré R, Gualtieri AF, Dražić G. 2019. Experimental quantification of the Fe-valence state at amosite-asbestos boundaries using acSTEM dual-electron energy-loss spectroscopy. Am Miner 104:1820–1828. https://doi.org/10.2138/am-2019-7218.
67. Vigliaturo R, Jamnik M, Dražić G, Podobnik M, Tušek Žnidarič M, Della Ventura G, Redhammer G, Žnidaršič N, Caserman S, Gieré R. 2022. Nanoscale transformations of amphiboles within human alveolar epithelial cells. Sci Rep 12:1782. https://doi.org/10.1038/s41598-022-05802-x.
68. Kato S, Hashimoto K, Watanabe K. 2012. Microbial interspecies electron transfer via electric currents through conductive minerals. Proc Natl Acad Sci U S A 109:10042–10046. https://doi.org/10.1073/pnas.1117592109.
69. Shi L, Dong H, Reguera G, Beyenal H, Lu A, Liu J, Yu H-Q, Fredrickson JK. 2016. Extracellular electron transfer mechanisms between microorganisms and minerals. Nat Rev Microbiol 14:651–662. https://doi.org/10.1038/nrmicro.2016.93.
70. Addison CC, Addison WE, Neal GH, Sharp JH. 1962. Amphiboles. Part I. The oxidation of crocidolite. J Chem Soc 1962:1468–1471. https://doi.org/10.1039/jr9620001468.
71. Addison WE, Sharp JH. 1962. Amphiboles. Part III. The reduction of crocidolite. J Chem Soc 1962:3693–3698.
72. Addison WE, Sharp JH. 1962. Redox behaviour of iron in hydroxylated silicates. Clays Clay Miner 11:95–104. https://doi.org/10.1346/CCMN.1962.0110110.
73. Gulumian M, Bhoolia DJ, Du Toit RSJ, Rendall REG, Pollak H, van Wyk JA, Rhempula M. 1993. Activation of UICC crocidolite: the effect of conversion of some ferric ions to ferrous ions. Environ Res 60:193–206. https://doi.org/10.1006/enrs.1993.1027.
74. Della VG, Mihailova B, Susta U, Guidi MC, Marcelli A, Schlüter J, Oberti R. 2018. The dynamics of Fe oxidation in riebeckite: a model for amphiboles. Am Min 103:1103–1111. https://doi.org/10.2138/am-2018-6382.
75. Littler JGF, Williams RJP. 1965. Electrical and optical properties of crocidolite and some other iron compounds. J Chem Soc 1965:6368–6371. https://doi.org/10.1039/jr9650006368.
76. Ballirano P, Bloise A, Gualtieri AF, Lezzerini M, Pacella A, Perchiazzi N, Dogan M, Dogan AU, Gualtieri AF. 2017. The crystal structure of mineral fibres, p 17– 64. *In* Gualtieri AF (ed), Mineral fibres: crystal chemistry, chemical-physical properties, biological interaction and toxicity. European Mineralogical Union and the Mineralogical Society, London, United Kingdom.
77. Hardy JA, Aust AE. 1995. Iron in asbestos chemistry and carcinogenicity. Chem Rev 95:97–118. https://doi.org/10.1021/cr00033a005.
78. Martra G, Chiardola E, Coluccia S, Marchese L, Tomatis M, Fubini B. 1999. Reactive sites at the surface of crocidolite asbestos. Langmuir 15:5742–5752. https://doi.org/10.1021/la9814541.
79. Schneider F, Sporn TA, Roggli VL. 2008. Crocidolite and mesothelioma. Ultrastruct Pathol 32:171–177. https://doi.org/10.1080/01913120802343848.
80. Garabrant DH, Pastula ST. 2018. A comparison of asbestos fiber potency and elongate mineral particle (EMP) potency for mesothelioma in humans. Toxicol Appl Pharmacol 15:127–136. https://doi.org/10.1016/j.taap.2018.07.003.
81. Hart HP. 1988. Asbestos in South Africa. J S Afr Inst Min Metall 88:185–198.
82. Harington JS, McGlashan ND. 1998. South African asbestos: production, exports, and destinations, 1959–1993. Am J Ind Med 33:321–326. https://doi.org/10.1002/(SICI)1097-0274(199804)33:4%3C321::AID-AJIM2%3E3.0.CO;2-X.
83. LaDou J, Castleman B, Frank A, Gochfeld M, Greenberg M, Huff J, Joshi TK, Landrigan PJ, Lemen R, Myers J, Soffritti M, Soskolne CL, Takahashi K, Teitelbaum D, Terracini B, Watterson A. 2010. The case for a global ban on asbestos. Environ Health Perspect 118:897–901. https://doi.org/10.1289/ehp.1002285.
84. Frank AL, Josgu TK. 2014. The global spread of asbestos. Ann Glob Health 80:257–262. https://doi.org/10.1016/j.aogh.2014.09.016.
85. Martra G, Tomatis M, Fenoglio I, Coluccia S, Fubini B. 2003. Ascorbic acid modifies the surface of asbestos: possible implications in the molecular mechanisms of toxicity. Chem Res Toxicol 16:328–335. https://doi.org/10.1021/tx0200515.
86. Gualtieri AF, Lusvardi G, Pedone A, Di Giuseppe D, Zoboli A, Mucci A, Zambon A, Filaferro M, Vitale G, Benassi M, Avallone R, Pasquali L, Lassinantti Gualtieri M. 2019. Structure model and toxicity of the product of biodissolution of chrysotile asbestos in the lungs. Chem Res Toxicol 32:2063–2077. https://doi.org/10.1021/acs.chemrestox.9b00220.
87. Hume LA, Rimstidt JD. 1992. The biodurability of chrysotile asbestos. Am Mineral 77:1125–1128.
88. Pacella A, Fantauzzi M, Turci F, Cremisini C, Montereali MR, Nardi E, Atzei D, Rossi A, Andreozzi GB. 2015. Surface alteration mechanism and topochemistry of iron in tremolite asbestos: a step toward understanding the potential hazard of amphibole asbestos. Chem Geol 405:28–38. https://doi.org/10.1016/j.chemgeo.2015.03.028.
89. Pacella A, Ballirano P, Fantauzzi M, Rossi A, Nardi E, Capitani G, Arrizza L, Montereali MR. 2021. Surface and bulk modifications of amphibole asbestos in mimicked Gamble's solution at acidic pH. Sci Rep 11:14249. https://doi.org/10.1038/s41598-021-93758-9.
90. Gronow JR. 1987. The dissolution of asbestos fibres in water. Clay Miner 22:21–35. https://doi.org/10.1180/claymin.1987.022.1.03.
91. Rozalen M, Huertas FJ. 2013. Comparative effect of chrysotile leaching in nitric, sulfuric and oxalic acids at room temperature. Chem Geol 352:134–142. https://doi.org/10.1016/j.chemgeo.2013.06.004.
92. Slobodkina GB, Kolganova TV, Querellou J, Bonch-Osmolovskaya EA, Slobodkin AI. 2009. Geoglobus acetivorans sp. nov., an iron(III)-reducing archaeon from a deep-sea hydrothermal vent. Int J Syst Evol Microbiol 59:2880–2883. https://doi.org/10.1099/ijs.0.011080-0.
93. Vetriani C, Speck MD, Ellor SV, Lutz RA, Starovoytov V. 2004. Thermovibrio ammonificans sp. nov., a thermophilic, chemolithotrophic, nitrate-ammonifying bacterium from deep-sea hydrothermal vents. Int J Syst Evol Microbiol 54:175–181. https://doi.org/10.1099/ijs.0.02781-0.
94. Vigliaturo R, Choi JK, Pérez-Rodríguez I, Gieré R. 2020. Dimensional distribution control of elongate mineral particles for their use in biological assays. MethodsX 7:100937. https://doi.org/10.1016/j.mex.2020.100937.
95. Stetter KO, König H, Stackebrandt E. 1983. Pyrodictium gen. nov., a new genus of submarine disc-shaped sulphur reducing archaebacteria growing optimally at 105°C. Syst Appl Microbiol 4:535–551. https://doi.org/10.1016/S0723-2020(83)80011-3.
96. Mohanty SK, Salamatipour A, Willenbring JK. 2021. Mobility of asbestos fibers below ground enhanced by dissolved organic matter from soil amendments. JHM Lett 2:100015.
97. Viollier E, Inglett PW, Hunter K, Roychoudhury AN, Van Cappellen P. 2000. The ferrozine method revisited: Fe(II)/Fe(III) determination in natural waters. Appl Geochem 15:785–790. https://doi.org/10.1016/S0883-2927(99)00097-9.
98. Stookey LL. 1970. Ferrozine—a new spectrophotometric reagent for iron. Anal Chem 42:779–781. https://doi.org/10.1021/ac60289a016.